nature neuroscience

Experience-dependent spatial expectations in mouse visual cortex

Aris Fiser[1,2,4], David Mahringer[1,2,4], Hassana K Oyibo[1,2,4], Anders V Petersen[3], Marcus Leinweber[1] & Georg B Keller[1,2]

In generative models of brain function, internal representations are used to generate predictions of sensory input, yet little is known about how internal models influence sensory processing. Here we show that, with experience in a virtual environment, the activity of neurons in layer 2/3 of mouse primary visual cortex (V1) becomes increasingly informative of spatial location. We found that a subset of V1 neurons exhibited responses that were predictive of the upcoming visual stimulus in a spatially dependent manner and that the omission of an expected stimulus drove strong responses in V1. Stimulus-predictive responses also emerged in V1-projecting anterior cingulate cortex axons, suggesting that anterior cingulate cortex serves as a source of predictions of visual input to V1. These findings are consistent with the hypothesis that visual cortex forms an internal representation of the visual scene based on spatial location and compares this representation with feed-forward visual input.

Evidence for the existence of internal representations of the environment in the brain has come, most prominently, from the discovery of spatial maps in the hippocampus and entorhinal cortex[1,2]. Visual cues exert a strong influence on the structure and arrangement of such maps[2,3]. Little is known, however, about how internal models of the environment influence sensory processing. Indirect evidence for an influence of internal representations on visual processing comes from the findings that hippocampal replay during sleep is accompanied by replay in visual cortex[4] and from the appearance of theta oscillations in the local field potential in visual cortices during locomotion in mice[5] and during short-term memory tasks in monkeys[6]. We speculated that if a direct influence of spatial maps on visual processing develops with experience, it could manifest as a prediction of visual stimulus based on spatial location. The underlying conceptual model is that spatial representations of the environment activate the corresponding visual representations of stimuli encountered in specific locations. This would likely be mediated by top-down projections to V1 from areas involved in spatial memory, like the anterior cingulate cortex (ACC)[7–10]. This leads to a number of testable predictions. First, visual representations of the environment should change systematically with increasing experience in a given environment. Second, we should find nonsensory stimulus-predictive responses that are tied to a conjunction of spatial location and the visual stimulus previously encountered at this location. Third, if the stimulus encountered at a given location is different from the one previously encountered at the same location, this should lead to detectable mismatch signals.

RESULTS

To probe for the existence of experience-dependent spatial expectations in mouse primary visual cortex, we repeatedly let mice explore a virtual tunnel over the course of several days. Throughout exploration, we chronically recorded the activity of the same 1,630 neurons in V1 layer 2/3 of nine adult C57BL/6 mice, using two-photon imaging of the genetically encoded calcium indicator GCaMP6f (expressed from the vector AAV2/1-Ef1a-GCaMP6f-WPRE; Online Methods)[11]. For all imaging experiments, mice were head-fixed and free to run on a spherical treadmill[12,13]. Rotation of the spherical treadmill was restricted to forward and backward directions, and it controlled movement in a virtual tunnel that was projected onto a toroidal screen surrounding the mouse (**Fig. 1a**). Upon reaching the end of the tunnel, mice received a water reward and their position was reset to the beginning of the tunnel. The walls of the virtual tunnel were lined with four different landmark stimuli and five uniform gray areas, marking locations at which one of two orthogonal sinusoidal gratings (henceforth referred to as A and B) were presented when the mouse reached the corresponding gray area (**Fig. 1b** and **Supplementary Video 1**). This was done to ensure precise control of when the mouse would first see the grating. During the first two sessions the sequence of the five grating stimuli was identical (A-B-A-B-A) on every traversal (condition 1). In subsequent sessions the identity of the last grating stimulus changed to a B on randomly selected traversals (90% A and 10% B in condition 2; 100% B in condition 3; and 10% A and 90% B in condition 4). In the fifth condition we omitted the grating in position 5 altogether on 10% of randomly selected traversals. Each condition comprised two recording sessions that lasted between 1 and 2 h and occurred daily (spaced by 24 ± 4 h, with the exception of condition 5, which immediately followed condition 4). We imaged from the same neurons chronically throughout the duration of the experiment. Animals traversed the tunnel an average of 109 times per session (**Supplementary Fig. 1a**). Each traversal lasted between 10 and 120 s (**Supplementary Fig. 1b**).

[1]Friedrich Miescher Institute for Biomedical Research, Basel, Switzerland. [2]Faculty of Natural Sciences, University of Basel, Basel, Switzerland. [3]Department of Neuroscience and Pharmacology, Faculty of Health and Medical Sciences, University of Copenhagen, Copenhagen, Denmark. [4]These authors contributed equally to this work. Correspondence should be addressed to G.B.K. (georg.keller@fmi.ch).

Received 16 May; accepted 8 August; published online 12 September 2016; doi:10.1038/nn.4385

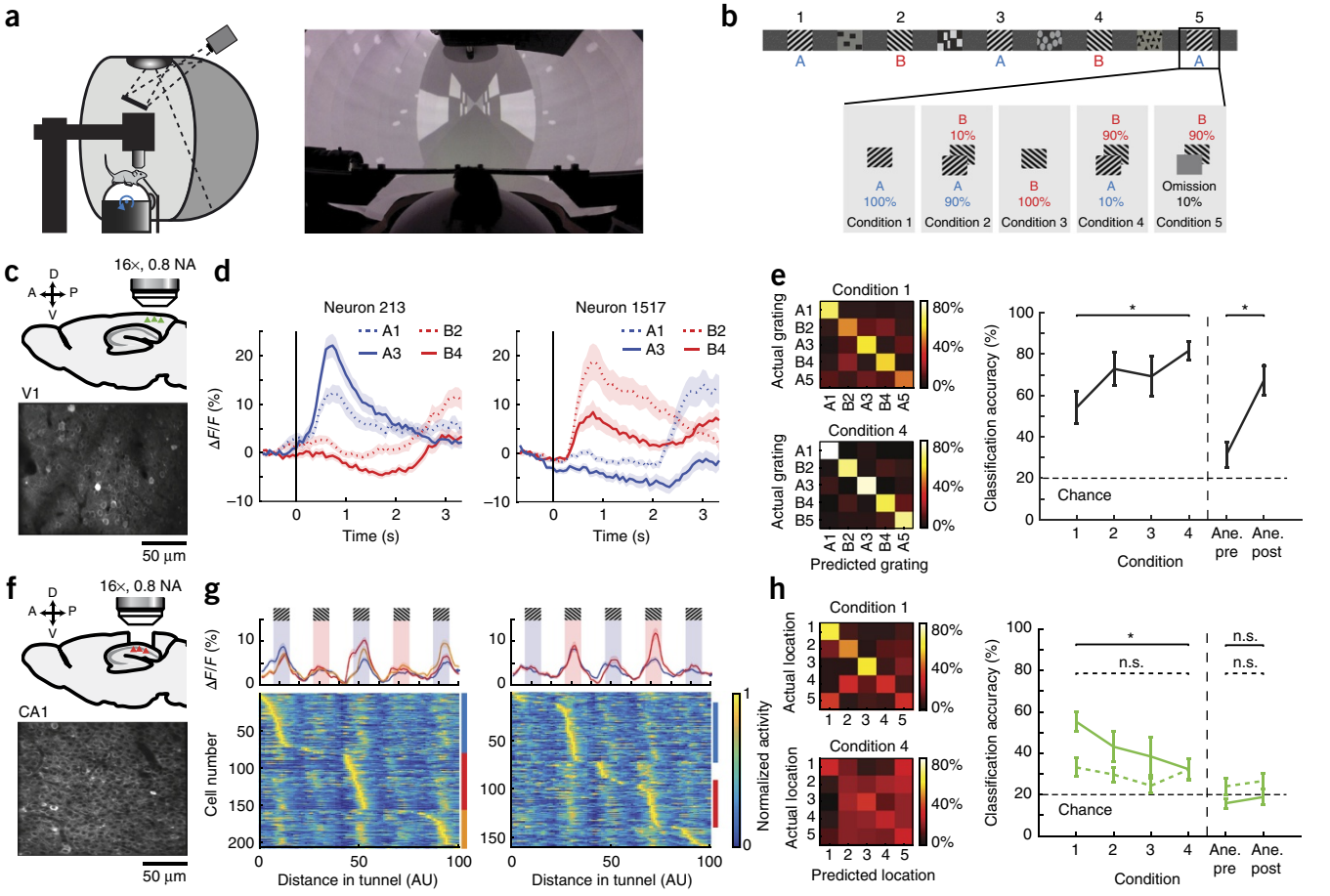

Figure 1 Identical visual stimuli in different spatial locations can elicit different responses in V1 and similar responses in CA1. (**a**) Left: schematic of the experimental setup. Right: photograph of a mouse approaching a landmark stimulus in the virtual tunnel. (**b**) Schematic representation of the texture lining both walls of the tunnel. Gratings A and B in positions 1–5 were only shown once the animal reached the corresponding position in the tunnel (**Supplementary Video 1**). In between the grating positions were four permanent landmark stimuli. The probability of encountering an A or B in position 5 changed with conditions as shown. (**c**) Top: schematic of V1 imaging strategy; NA, numerical aperture. Bottom: example two-photon image of V1 layer 2/3 neurons. (**d**) Average responses of an example A-selective neuron (left) and an example B-selective neuron (right) to A1, B2, A3 and B4. Note that the responses to the preferred stimulus depend on where in the tunnel the stimulus is encountered (position 1 versus 3 or position 2 versus 4). Shading indicates s.e.m. across grating presentations (left: 178 presentations; right: 218 presentations). (**e**) Classification accuracy of grating location and identity based on neural activity increases with experience. Left: confusion matrices of the distributions of classified grating location (*x* axis) based on grating onset responses as a function of actual grating location (*y* axis). Right: mean classification accuracy for all conditions, measured as the mean of the diagonal of the confusion matrix for each condition. Note that for these plots, V1 data recorded in conditions 1–2 (from 9 animals) and data recorded in conditions 1–4 (from 6 animals) were combined. Error bars: mean ± s.e.m. across animals. $^*P = 0.029$ (conditions 1 and 4); $P = 0.031$ (Ane. pre and Ane. post), Wilcoxon rank-sum test. (**f**) Top: schematic of CA1 imaging strategy. Bottom: example two-photon image of CA1 pyramidal neurons. (**g**) Heat maps showing normalized fluorescence traces of CA1 neurons in condition 1, selective for A (left) and B (right), sorted by peak position. Traces on top are the mean activity of neurons shown below, highlighted by the blue, red and orange vertical bars. AU, arbitrary units. (**h**) Left: as in **e**, but based on mean response, not grating onset response. Right: as in **e**, for mean response (solid line) and for grating onset response (dashed line). Error bars: mean ± s.e.m. across animals ($n = 5$). $^*P = 0.043$, n.s.: $P = 0.931$ (conditions 1 and 4); n.s.: $P = 0.524$, $P = 0.463$ (Ane. pre and Ane. post); Wilcoxon rank-sum test.

In addition, we measured responses of the same neurons during anesthesia to passive presentations of the tunnel presented at a constant visual flow speed both before the first condition ('pre-experience anesthesia') and after the last condition ('post-experience anesthesia'). In total we recorded the activity of 1,147 L2/3 neurons in V1 of six animals exposed to conditions 1 through 5 (**Fig. 1b**), of which 899 neurons were responsive to at least one visual element of the tunnel (tunnel-responsive, 78.4%; Online Methods). We also recorded from 483 neurons in conditions 1 and 2 in three more animals; of these, 436 neurons were classified as tunnel responsive (90.2%; in total, 1,335 of 1,630, or 81.9%, of neurons were tunnel-responsive).

To compare dynamics of spatial signals in V1 to potential changes in the spatial map in hippocampus, we chronically recorded the activity of the same 1,736 neurons in hippocampal region CA1 in 5 animals exposed to conditions 1 through 5 (**Supplementary Fig. 2a** and **Supplementary Video 2**; Online Methods). Changes in spatial signals in V1 could be the result of changes in the spatial representation in hippocampus or in the way V1 is activated by the spatial representation. In either case, these changes should be reflected in top-down inputs to V1. One of the candidate structures for such top-down inputs to V1 is the ACC. ACC is known to project to V1 (refs. 14–16) and has been shown to be involved in long-term memory storage[7–10]. To test whether spatial information could be relayed to V1 via ACC, we recorded the activity of ACC axons in layer 1 of V1 in condition 1 (3,513 axons, 5 sites) and in condition 4 (8,599 axons, 10 sites) in 5 animals (Online Methods). Note that, unlike in the V1 and CA1 experiments, we were unable to

chronically record from the same ACC axons on different days. The combination of the high density of ACC axons in layer 1 of V1 and the low baseline fluorescence made it impossible for us to ensure that we were recording from the same axons on different days. However, there likely was a large overlap between the axons recorded on different days as imaging regions (5 of 10) were realigned based on blood vessel patterns (**Supplementary Fig. 2b** and **Supplementary Video 3**). We imaged activity on the first and the sixth day (2 sites, 1 animal) or seventh day (8 sites, 4 animals) in the tunnel. As the total experience in the tunnel between the two imaging time points was comparable to the difference between condition 1 and condition 4 in the V1 and CA1 data, we will use the same nomenclature for the ACC data.

V1 activity becomes descriptive of spatial location

To probe for a spatial component in V1 activity, we investigated whether location in the environment modulated neuronal responses to identical visual stimuli. We found that peak calcium fluorescence amplitudes of grating-responsive neurons were different for the presentation of the same grating in different positions in the tunnel (**Fig. 1c**,**d**). To quantify the spatial heterogeneity of neuronal responses in the population, we trained a classifier (Matlab TreeBagger; Online Methods) to predict which grating location the mouse was traversing in each trial for each behavioral condition using the average population activity within a 667-ms (10-frame) window following each grating onset. Based on V1 activity, the classifier was able to predict not only the identity of the grating the mouse was seeing but also where in the tunnel the mouse was seeing the grating (**Fig. 1e**). Classification performance, measured as the mean of the diagonal of the confusion matrix for each condition (Online Methods), significantly increased between conditions 1 and 4 (condition 1: 53.3% ± 7.7% correct; condition 4: 81.7% ± 4.6% correct, mean ± s.e.m.; $P = 0.029$; Wilcoxon rank-sum test). The classifier also performed considerably better in post-experience anesthesia ('Ane. Post') compared to pre-experience anesthesia (Ane. Post; **Fig. 1e** and **Supplementary Fig. 3a**; Ane. Pre: 31.3% ± 6.2% correct; Ane. Post: 67.2% ± 7.2% correct; $P = 0.031$; Wilcoxon rank-sum test). To ensure that the difference in responses to the same stimulus in different locations was not due to running speed tuning[5,17], we trained a classifier to predict the animal's location based on running speed. The classifier did not perform better than chance (**Supplementary Fig. 3b**). Training a classifier on slow traversals and testing it on fast traversals, and vice versa, yielded classification accuracy that remained well above chance in both cases (**Supplementary Fig. 3c**), suggesting that speed tuning is not a major contributor of predictive power in the classification. To test whether calcium dynamics influence the change in classification performance, we deconvolved raw calcium traces using an exponential kernel with a time constant of 0.5 s (**Supplementary Fig. 3d** and Online Methods)[11,18] and trained the classifier on the deconvolved traces. Average accuracy was slightly decreased when the classifier was trained on deconvolved traces, but the increase between condition 1 and 4 was unchanged (**Supplementary Fig. 3e**).

In addition to a spatial component in V1 activity, an increase in stimulus selectivity could also influence the discriminability of stimuli in the environment. We quantified the selectivity of all neurons to the two grating stimuli A and B using a selectivity index (SI) defined as $(R_A - R_B)/(R_A + R_B)$, where R_A is the average response to A in positions 1 and 3, and R_B is the average response to B in positions 2 and 4; SI was set to 0 for neurons without a significant response to either A or B (**Supplementary Fig. 4a** and Online Methods). We found that, with experience, neurons in V1 that were grating-selective became more selective with time (**Supplementary Fig. 4b**,**c**), an effect that cannot be explained by their mean activity (**Supplementary Fig. 4e**). Furthermore, the stability of these selective neurons increased with experience, an effect not explained by stability in motor behavior (**Supplementary Fig. 4f**).

Activity in CA1 exhibited place-like responses that reflected the pattern of visual stimuli along the tunnel. Neurons responded to either landmark stimuli or gratings, and locations with similar visual stimuli elicited similar neural responses (**Fig. 1f**,**g** and **Supplementary Fig. 5a**), with no clear anatomical clustering in CA1 of neurons that responded to gratings or landmarks (**Supplementary Fig. 5b**,**c**). Consistent with previous reports[19], we found that activity patterns were only partially stable over different conditions or days. For 14.8% of neurons, the location of peak activity in the tunnel was stable over the five behavioral conditions (within 5% of tunnel length; **Supplementary Fig. 6a**,**c** and Online Methods). By comparison, in V1, 32% of neurons exhibited a stable location of peak activity (**Supplementary Fig. 6b**,**c**). The instability of CA1 activity may have been augmented by the unilateral removal of cortical tissue necessary to image CA1 pyramidal neurons. Previous work, however, has argued that place field responses measured by imaging using similar methods are not different from those measured with electrophysiological techniques[20]. Classification of grating identity based on grating onset responses using CA1 data was only slightly above chance (**Fig. 1h**). This was likely due to the absence of clear grating onset responses (**Fig. 1g**); using mean activity instead of grating onset responses, classification performance in condition 1 was not different from that based on V1 data. However, classification performance decreased with experience, indicating that CA1 activity becomes less informative of spatial location (**Fig. 1h**; condition 1: 53.9% ± 4.4%; condition 4: 32.3% ± 4.8%; mean ± s.e.m.; $P = 0.043$; Wilcoxon rank-sum test). Furthermore, neurons that were stimulus-selective on average showed decreasing selectivity with experience and maintained high trial-to-trial response variability (**Supplementary Fig. 4d–f**). This is the opposite of the trend we observed in V1 activity, where decoding performance increased with experience. The experience-dependent effects found in V1 therefore cannot be explained by a concurrent change of a spatial map in CA1.

V1 develops predictive responses to upcoming visual stimuli

A potential role for the spatial modulation of V1 activity is to enhance the discriminability of similar stimuli in different contexts. In this scenario, a spatial input would trigger predictions of expected visual input at a given spatial position. Indeed, we found a group of neurons (5.6%, or 50 of 899 tunnel-responsive neurons) that, with increasing experience in the tunnel, started firing before the appearance of the upcoming grating in an A- or B-selective manner (**Fig. 2a**,**b**). As responses both preceded the stimulus and signaled the identity of the upcoming stimulus, we will refer to these signals as stimulus-predictive. The response in predictive neurons developed with experience and was absent in the first condition (**Fig. 2b**) and during anesthesia (**Supplementary Fig. 7a**). In contrast, responses in neurons classified as visual and selective to either A or B (4.9%, or 44 of 899 tunnel-responsive neurons) were present already in the first condition and exhibited a much smaller increase with experience (**Fig. 2c**). Predictive and visual neurons were equally selective for A or B (**Supplementary Fig. 7b**; predictive neurons: mean SI = 0.79 ± 0.04; visual neurons: 0.82 ± 0.03). Using a classifier trained on the activity of predictive neurons preceding the appearance of the stimulus, we were able to predict the identity of the upcoming visual stimulus (**Fig. 2d**; accuracy = 81.4 ± 5.1%, mean ± s.e.m.). Once present, predictive responses were stable over conditions. The correlation of the mean responses of predictive neurons between conditions 3 and 4 was almost as high as for visual neurons (predictive neurons: $r = 0.81$, $P = 1.1 \times 10^{-27}$; visual

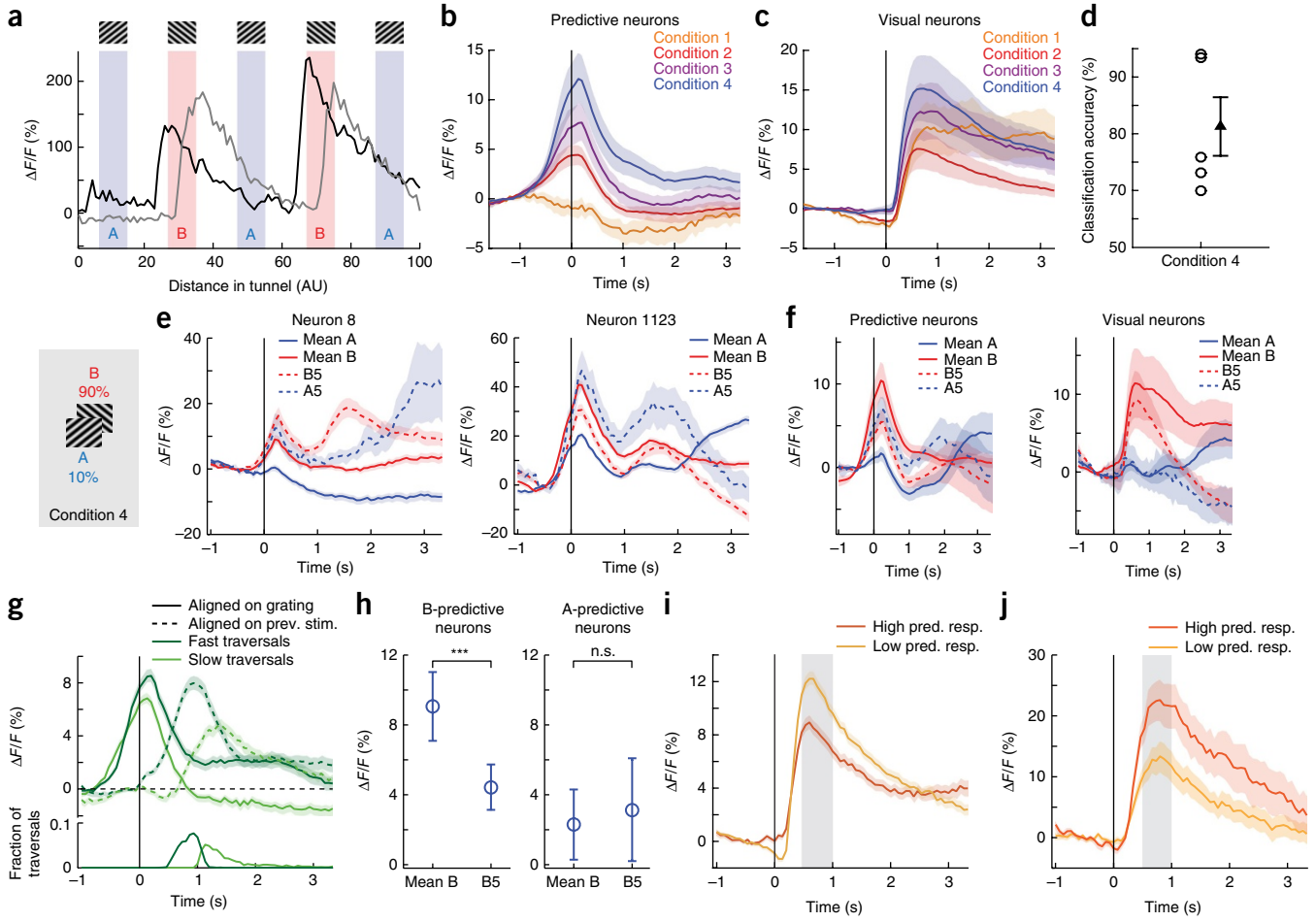

Figure 2 V1 neurons develop predictive responses to approaching visual stimuli with experience. (**a**) The activity of two B-selective neurons during a single traversal of the tunnel. Note that one neuron (black line) fires in anticipation of each B presentation, whereas the other fires causally with a delay after the presentation. (**b**,**c**) The average response of predictive (**b**; 50 neurons) and visual (**c**; 44 neurons) stimulus-selective neurons to their preferred grating orientation in conditions 1–4. In these and all following panels, shading along curves indicates s.e.m. (**d**) Classification accuracy of a classifier trained on the activity of predictive neurons ($n = 50$) to decode grating identity (A3 vs. B4) before the stimulus (–333 ms to 0 ms). Circles: individual sites (5 sites); triangle: mean; error bars: s.e.m. Data in **d**–**i** are from condition 4. (**e**) Average responses of two example B-selective neurons to mean A1 and A3 (blue solid line), mean B2 and B4 (red solid line), unexpected A5 (blue dashed line), and expected B5 (red dashed line). (**f**) Average responses of predictive ($n = 50$) and visual ($n = 44$) neurons to mean A1 and A3, mean B2 and B4, expected B5 and unexpected A5. (**g**) Top: responses of predictive neurons ($n = 50$) aligned to either previous landmark stimulus (dashed lines) or upcoming grating stimulus (solid lines) for fast (dark green) and slow traversals (light green). Responses for slow and fast traversals align best with upcoming grating onset. Bottom: histogram of time between previous landmark stimulus and upcoming grating onset for fast (dark green) and slow (light green) traversals. Fast and slow traversals were classified by mean running speed in a window of 467 ms (7 frames) preceding onset of the grating stimulus. (**h**) Strength of predictive responses of B-predictive neurons ($n = 39$, left) and A-predictive neurons ($n = 11$, right) to B2 and B4 (mean B) and B5 in condition 4, where the animal always encountered B in positions 2 and 4 but had only a 90% of encountering it in position 5. Error bars: mean ± s.e.m. across neurons. (***$P = 0.00015$, n.s.: $P = 0.7$; Wilcoxon signed-rank test). (**i**) Responses of visual neurons on traversals of high (orange) and low (yellow) activity in predictive neurons. Strong predictive activity before a grating (in the top 20%, 787 grating presentations) correlated with weak visually driven responses, and vice versa (in the bottom 20%, 787 grating presentations). Mean responses are calculated in the window indicated with gray shading. (**j**) Average responses of visual A-selective neurons in response to the unexpected A5 in traversals with weak (yellow; 51 A5 presentations) and strong (orange; 52 A5 presentations) activity in predictive B-selective neurons. The higher the activity in predictive B-selective neurons, the higher the mean visual responses to the unexpected A (mean responses were calculated in the window indicated with gray shading).

neurons: $r = 0.95$, $P = 5.4 \times 10^{-47}$). Moreover, only one neuron classified as predictive in condition 3 was classified as visual in condition 4.

In conditions 2 and 4 we presented a different grating on 10% of randomly selected traversals in the final location (**Fig. 1b**). On these traversals, with an unexpected grating in the final location, stimulus-predictive neurons fired as if the predicted grating would appear but visual neurons fired in response to the actual grating shown (**Fig. 2e**,**f**). Predictive responses to an unexpected A (A5) were also apparent when plotting the average response of the 20% ($n = 229$) of neurons that responded most strongly to an expected B (**Supplementary Fig. 7c**). Given that stimulus-predictive neurons were as selective for the upcoming stimulus (A or B) on average as visual neurons, it is unlikely that predictive responses are responses to the preceding stimulus. To confirm this, we aligned responses of stimulus-predictive neurons to either the preceding landmark stimulus or the upcoming grating for fast and slow traversals separately. Alignment of the responses for fast and slow traversals should be best for the stimulus (previous or upcoming) that actually drives the responses. We found

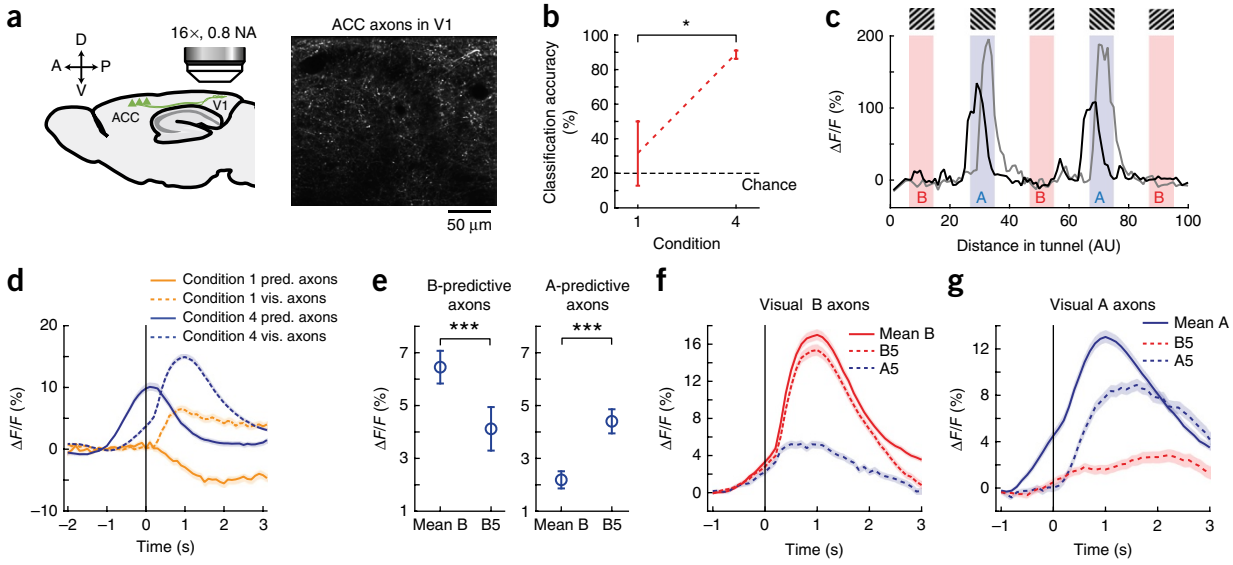

Figure 3 ACC projections to V1 carry visual stimulus predictions. (**a**) Left: schematic of ACC axon imaging strategy. Right: example two-photon image of ACC axons in V1. (**b**) Classification accuracy for a classifier trained to decode grating location based on grating onset responses (as in **Fig. 1e**,**h**). The accuracy of the classifier increases with time. Mean ± s.e.m. across sites (condition 1: 3 sites; condition 4: 10 sites). $^{*}P = 0.03$, Wilcoxon rank-sum test. (**c**) Activity of two A-selective axons during a single traversal of the tunnel. One axon (black line) fires in anticipation of each A, whereas the other (gray line) peaks after each stimulus. (**d**) As in V1, stimulus-predictive responses in ACC emerge with experience. Orange lines indicate mean activity of predictive (solid; $n = 654$) and visual (dashed; $n = 1{,}377$) axons in condition 1, whereas blue lines indicate activity of the corresponding axons in condition 4 (736 predictive and 2,559 visual axons). Shading indicates s.e.m. across axons. Pred., predictive; vis., visual. (**e**) As in **Figure 2h**, for V1-projecting ACC axons. Strength of predictive responses of B-predictive axons (left) and A-predictive axons (right) to B2 and B4 (mean B) and B5 in condition 4, where the animal always encountered B in position 2 and 4 but had only a 90% of encountering it in position 5. Mean ± s.e.m. across axons (312 A-predictive and 500 B-predictive axons). $^{***}P = 0.00015$ (A-predictive), $P = 0.00028$ (B-predictive), Wilcoxon signed-rank test. (**f**) Activity of visual B axons ($n = 1{,}175$) to mean B (B2 and B4) (solid red line), expected B5 (dashed red line) and unexpected A5 (dashed blue line). (**g**) As in **f**, but for visual A axons ($n = 1{,}384$). Note the visually evoked response to the unexpected A5. Shading in **f** and **g** indicates s.e.m.

that responses were best aligned with the upcoming stimulus (**Fig. 2g**) and thus are best explained by distance, not time, from the last stimulus. This implies that predictive activity relies on spatial location to signal the upcoming visual stimulus.

Stimulus-predictive signals could reflect the frequency of having encountered a certain stimulus in a specific location. Thus predictive signals should be higher when the same stimulus is always encountered as opposed to when, in a specific location, different stimuli were encountered during experience. Therefore, the predictive response to B5 should be lower than the predictive response to mean B, as the stimulus presented in position 5 varied with session (**Fig. 1b**), whereas in position 2 and 4 the animal always encountered a B. This was indeed the case: in condition 4, B-selective predictive neurons were significantly less active before grating B5 (90% B) than on average to gratings B2 and B4 (100% B) (**Fig. 2h**; mean B: $\Delta F/F = 9.1\% \pm 2\%$; B5: $\Delta F/F = 4.4\% \pm 1.3\%$; $P = 0.00015$, Wilcoxon signed-rank test). Conversely, one could argue that A-predictive neurons should be more active before B5 because the animal encounters an A in this location on 10% of the traversals. A rare encounter, however, did not lead to a measureable increase in predictive activity in V1 (**Fig. 2h**; mean B: $\Delta F/F = 2.3\%$; ± 2% B5: $\Delta F/F = 3.1\% \pm 2.9\%$; $P = 0.7$, Wilcoxon signed-rank test).

In predictive coding models, the primary visual cortex communicates the error between predicted and actual visual stimuli to downstream visual areas[21,22]. If predictive activity scales with the frequency of having encountered a visual stimulus in a particular location, then the strength of the visual response to the stimulus may signal the surprise of seeing it. This would be reflected in lower visually driven activity on trials when prediction of a grating was high. We observed that on traversals with high predictive activity preceding each grating, visually evoked activity to the grating was lower ($\Delta F/F = 8.0\% \pm 0.5\%$, mean ± s.e.m.) than on traversals with low predictive activity ($\Delta F/F = 11.2\% \pm 0.5\%$, mean ± s.e.m.; **Fig. 2i** and **Supplementary Fig. 7d**). In sum, this suggests that stronger visual responses report the discrepancy between predicted and actual visual input and that activity in stimulus-predictive neurons may lead to a reduction in visual responses.

If activity in stimulus-predictive neurons indeed signals the identity of the upcoming stimulus, one would expect a difference in the visual response when an unpredicted stimulus is encountered. We found that the responses of A-selective visual neurons to the unexpected A at position 5 were stronger when B-predictive neurons fired strongly in anticipation to the grating presentation (**Fig. 2j**). Traversals were split into two groups by median amplitude of the response of predictive neurons (average visual responses on traversals with high predictive activity: 21.4% ± 3.1% $\Delta F/F$; and on traversals with low predictive activity 12.5% ± 2.2% $\Delta F/F$; mean ± s.e.m.; $P = 0.02$, Wilcoxon rank-sum test). Altogether, these findings indicate that the strength of predictive responses preceding a stimulus strongly affects the visual responses to it, suggesting a dynamic interplay between stimulus prediction and stimulus response.

ACC conveys stimulus predictive signals to V1

As the source of predictive signals must be extra-retinal, one would expect that at least some of the top-down inputs to primary visual cortex will exhibit stimulus-predictive signals and that this predictive input will develop with experience. To test this, we imaged from ACC axons in V1 (**Fig. 3a**). When classifying grating position based on the activity of ACC axons, we found an increase in classification accuracy with experience, similar to the increase in V1 (**Fig. 3b**; condition

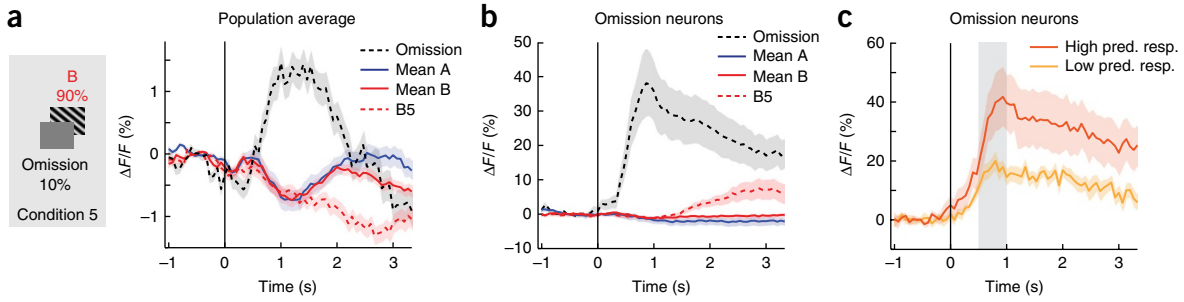

Figure 4 The omission of an expected grating strongly drives activity in V1. (**a**) Average population response (1,147 neurons) to the omission of grating B5 (black dashed line) in comparison to the average response to A (blue line), B (red line) and B5 (red dashed line). Shading indicates s.e.m. across neurons. (**b**) As in **a**, but for omission-selective neurons (21 of 899 tunnel-responsive neurons). Shading indicates s.e.m. across neurons. (**c**) Average omission responses in omission-selective neurons on traversals of high activity in predictive neurons (orange line; 13 traversals) and on traversals with low activity in predictive neurons (yellow line; 12 traversals). Gray shading indicates window over which mean activity was calculated. Shading indicates s.e.m. over traversals.

1: 31.7 ± 18.3%; condition 4: 88.6 ± 2.4%, mean ± s.e.m.; $P = 0.03$, Wilcoxon rank-sum test). We then compared the activity of ACC axons that exhibited selective responses for either A or B in early and late conditions. Using the same criteria as for responses in V1 (**Fig. 2b**,**c**) we were able to classify axons as either predictive or visual in both early and late conditions (**Fig. 3c**,**d**). We found there were visual responses but no predictive responses in early conditions and that stimulus-predictive responses emerged in late conditions (**Fig. 3d**). Notably, even axons classified as visual exhibited activity that preceded the presentation of the stimulus in condition 4. The contribution of these predictive responses to the total population response to gratings was larger in ACC than in V1 (**Supplementary Fig. 7e**). As in V1 (**Fig. 2h**), the strength of predictive responses depended on the reliability of having encountered a certain stimulus in a specific location. Predictive responses to B2 and B4 (100% B) were larger than predictive responses to B5 (90% B and 10% A in condition 4; mean B: $\Delta F/F = 6.5\% \pm 0.6\%$; B5: $\Delta F/F = 4.2\% \pm 0.8\%$; mean ± s.e.m.; $P = 0.00028$, Wilcoxon signed-rank test) and, in contrast to activity in V1, A-predictive activity was higher before B5 than before B2 and B4 (**Fig. 3e**; mean B: $\Delta F/F = 2.2\% \pm 0.3\%$; B5: $\Delta F/F = 4.4\% \pm 0.5\%$; mean ± s.e.m.; $P = 0.00015$, Wilcoxon signed-rank test).

Predictive inputs from ACC could signal spatial location (in spatial coordinates) or signal the predicted visual stimulus (in visual coordinates). To test whether axons classified as visual in condition 4 were actually visually driven, we compared responses of expected and unexpected presentations of A or B (condition 4). Axons that were B-selective had visual responses to an expected B5 comparable to the mean response to B. Responses to the unexpected A still showed predictive activity but diverged from B responses following stimulus onset (**Fig. 3f**). Conversely, axons selective for A exhibited predictive responses to an expected A1 or A3 and only small responses to the expected B5 but showed clear visual responses to the unexpected A5 (**Fig. 3g**). Thus, predictive signals in V1 are likely conveyed by top-down signals carrying an expectation of the visual input based on spatial location.

Omitting an expected stimulus drives strong responses in V1

To probe whether expectations can drive responses in V1 in the absence of a visual stimulus, we omitted the final stimulus altogether in 10% of randomly selected traversals (condition 5). In these omission traversals, no grating would appear as the mouse reached the gray area marking the location of the final grating presentation (**Supplementary Video 1**). The omission of the stimulus elicited a strong response in the V1 population (**Fig. 4a**, **Supplementary Fig. 8a** and **Supplementary Video 4**). Moreover, a subset of neurons selectively responded to the omission (**Fig. 4b**; 2.3%, or 21 of 899 tunnel-responsive neurons). If this omission response indeed signals a deviation between predicted and actual visual input, one would expect the strength of the predictive response to correlate with the omission response. To test this, we split all traversals into two categories depending on how strong the average response of predictive A- and B-selective neurons was before the omission. The average omission response in trials with low predictive activity was significantly smaller than in trials with high predictive activity (**Fig. 4c**; omission-evoked activity on trials with high predictive activity: $\Delta F/F = 35.2\% \pm 8.5\%$; on trials with low predictive activity: $\Delta F/F = 16.6\% \pm 2.2\%$, mean ± s.e.m.; $P = 0.00018$, Wilcoxon rank-sum test with bootstrapping; Online Methods). The lack of local visual flow during the grating omissions raises the possibility that these responses are instances of sensorimotor mismatch[17]. To test this, we compared the omission responses of the omission-selective neurons to their responses to the expected uniform gray stimulus that the animals encountered while running at the beginning and end of the tunnel. We found no response to the expected gray stimulus in omission-selective neurons (**Supplementary Fig. 8b**). Thus, omission responses can best be explained by a deviation between expected and actual visual stimulus based on what the mouse had seen in this position on previous traversals. Furthermore, omission responses were absent in ACC axons (**Supplementary Fig. 8c**), suggesting that visual cortex compares visual stimulus predictions, relayed by top-down cortical input, to actual visual input.

DISCUSSION

In this study, we found that the activity of neurons in the primary visual cortex of the mouse is shaped by experience. The increase in selectivity and trial-to-trial stereotypy of stimulus-selective neurons suggests that the representation of an environment in visual cortex is dynamic and becomes increasingly stable with experience. The emergence of stimulus-predictive activity with experience and the presence of an error signal in response to an unexpected stimulus, the strength of which correlates with the strength of the predictive activity preceding it, indicate that processing in V1 in a familiar environment relies on predictions of visual stimuli. These findings build upon previous work on internal representations showing that motor-related signals are integrated with sensory signals in primary sensory cortices to generate sensorimotor-mismatch signals[17,23–25].

Our results cannot be explained by timing-dependent recall of activity or reward anticipation. Cue-triggered recall of activity, for example, has been shown to occur in visual cortex after repeated experience of rapid sequences of stimuli[26] and fast-moving spots[27]. Sequence learning, however, is specific to the timing used for training; a change in timing of the stimuli of as little as 150 ms abolishes the effect[26]. Predictive responses in our experiments persisted even though trial-to-trial differences

in traversal times were on the order of tens of seconds (**Fig. 2g** and **Supplementary Fig. 1b**). Moreover, the cue-triggered recall was only observed when the animal was anesthetized or the animal was awake but cortex was in a synchronized state (characteristic of quiet wakefulness); the effect was absent when cortex was in a desynchronized state (characteristic of motor behavior)[27]. Another effect that has been shown to drive activity in visual cortex is reward anticipation[28]. Neurons that encode a rewarded stimulus are selectively activated in anticipation of reward-predicting stimuli[29]. However, as predictive activity in our data is stimulus-selective and omission responses are independent of the reward delivered at the end of the tunnel, reward anticipation cannot explain the spatial modulation we describe here.

The decrease we observed in spatial information in CA1 with experience implies that the experience-dependent effects found in V1 do not merely reflect a concomitant change in the hippocampal formation. Rather, place-like responses in CA1, which are tied to visual elements of the virtual tunnel, could serve as a scaffold for spatially modulated and stimulus-predictive activity in higher cortical areas that is then relayed to V1 via top-down input. We note that decoding of spatial location based on CA1 activity resulted in poorer accuracy than decoding of spatial location based on V1 activity. This could be a direct consequence of the virtual environment and head fixation or due to the fact that, to image CA1, we removed a part of visual cortex above CA1. Note, however, that one of the main factors contributing to poor decoding of spatial location from CA1 activity was the fact that CA1 neurons responded in multiple visually identical locations. It is unlikely that this is the result of damage to visual cortex. Lastly, although the head fixation and navigation in a virtual environment degrade the spatial representation in CA1 (ref. 30), this did not affect our ability to decode spatial information from V1 and ACC activity after experience.

Direct projections from cortical areas containing spatial representations of the environment, such as the retrosplenial cortex[31,32] or ACC[33], exist in rodent V1 (refs. 14–16). We found that one of these top-down projections carries a prediction of visual stimulus based on the mouse's location in the environment. Top-down mediated predictions could be compared against feed-forward sensory input to compute deviations between actual and predicted sensory input, and such deviations could be used to update expectations and guide learning. Our results are consistent with a predictive coding framework, in which sensory input is compared to an internal model of the environment to detect deviations from expectations.

METHODS

Methods, including statements of data availability and any associated accession codes and references, are available in the online version of the paper.

Note: Any Supplementary Information and Source Data files are available in the online version of the paper.

ACKNOWLEDGMENTS

We thank T. Mrsic-Flogel, E. Feinberg and A. Lüthi for discussion of and comments on earlier versions of this manuscript. We thank D. Gerosa-Erni for production of the AAV vectors, B. Wang for help with the construction of the microscope and virtual reality setup, and the members of the Keller laboratory for discussion and support. This work was supported by the Swiss National Science Foundation, the Novartis Research Foundation and the Human Frontier Science Program, and by a PhD fellowship from the Boehringer Ingelheim Fonds (A.F.).

AUTHOR CONTRIBUTIONS

A.F., D.M. and H.K.O. performed the V1 experiments. D.M., A.F. and A.V.P. performed the CA1 experiments. M.L. performed the ACC experiments. A.F. analyzed the V1 data. A.F. and A.V.P. analyzed the CA1 data. A.F. and M.L. analyzed the ACC data. A.F., D.M., H.K.O. and G.B.K. wrote the manuscript.

COMPETING FINANCIAL INTERESTS

The authors declare no competing financial interests.

1. O'Keefe, J. & Dostrovsky, J. The hippocampus as a spatial map. Preliminary evidence from unit activity in the freely-moving rat. *Brain Res.* **34**, 171–175 (1971).
2. Hafting, T., Fyhn, M., Molden, S., Moser, M.-B. & Moser, E.I. Microstructure of a spatial map in the entorhinal cortex. *Nature* **436**, 801–806 (2005).
3. O'Keefe, J. & Conway, D.H. Hippocampal place units in the freely moving rat: why they fire where they fire. *Exp. Brain Res.* **31**, 573–590 (1978).
4. Ji, D. & Wilson, M.A. Coordinated memory replay in the visual cortex and hippocampus during sleep. *Nat. Neurosci.* **10**, 100–107 (2007).
5. Niell, C.M. & Stryker, M.P. Modulation of visual responses by behavioral state in mouse visual cortex. *Neuron* **65**, 472–479 (2010).
6. Lee, H., Simpson, G.V., Logothetis, N.K. & Rainer, G. Phase locking of single neuron activity to theta oscillations during working memory in monkey extrastriate visual cortex. *Neuron* **45**, 147–156 (2005).
7. Frankland, P.W., Bontempi, B., Talton, L.E., Kaczmarek, L. & Silva, A.J. The involvement of the anterior cingulate cortex in remote contextual fear memory. *Science* **304**, 881–883 (2004).
8. Maviel, T., Durkin, T.P., Menzaghi, F. & Bontempi, B. Sites of neocortical reorganization critical for remote spatial memory. *Science* **305**, 96–99 (2004).
9. Teixeira, C.M., Pomedli, S.R., Maei, H.R., Kee, N. & Frankland, P.W. Involvement of the anterior cingulate cortex in the expression of remote spatial memory. *J. Neurosci.* **26**, 7555–7564 (2006).
10. Weible, A.P., Rowland, D.C., Monaghan, C.K., Wolfgang, N.T. & Kentros, C.G. Neural correlates of long-term object memory in the mouse anterior cingulate cortex. *J. Neurosci.* **32**, 5598–5608 (2012).
11. Chen, T.-W. *et al.* Ultrasensitive fluorescent proteins for imaging neuronal activity. *Nature* **499**, 295–300 (2013).
12. Hölscher, C., Schnee, A., Dahmen, H., Setia, L. & Mallot, H.A. Rats are able to navigate in virtual environments. *J. Exp. Biol.* **208**, 561–569 (2005).
13. Dombeck, D.A., Khabbaz, A.N., Collman, F., Adelman, T.L. & Tank, D.W. Imaging large-scale neural activity with cellular resolution in awake, mobile mice. *Neuron* **56**, 43–57 (2007).
14. Vogt, B.A. & Miller, M.W. Cortical connections between rat cingulate cortex and visual, motor, and postsubicular cortices. *J. Comp. Neurol.* **216**, 192–210 (1983).
15. Miller, M.W. & Vogt, B.A. Direct connections of rat visual cortex with sensory, motor, and association cortices. *J. Comp. Neurol.* **226**, 184–202 (1984).
16. Zhang, S. *et al.* Selective attention. Long-range and local circuits for top-down modulation of visual cortex processing. *Science* **345**, 660–665 (2014).
17. Keller, G.B., Bonhoeffer, T. & Hübener, M. Sensorimotor mismatch signals in primary visual cortex of the behaving mouse. *Neuron* **74**, 809–815 (2012).
18. Yaksi, E. & Friedrich, R.W. Reconstruction of firing rate changes across neuronal populations by temporally deconvolved Ca2+ imaging. *Nat. Methods* **3**, 377–383 (2006).
19. Ziv, Y. *et al.* Long-term dynamics of CA1 hippocampal place codes. *Nat. Neurosci.* **16**, 264–266 (2013).
20. Dombeck, D.A., Harvey, C.D., Tian, L., Looger, L.L. & Tank, D.W. Functional imaging of hippocampal place cells at cellular resolution during virtual navigation. *Nat. Neurosci.* **13**, 1433–1440 (2010).
21. Rao, R.P.N. & Ballard, D.H. Predictive coding in the visual cortex: a functional interpretation of some extra-classical receptive-field effects. *Nat. Neurosci.* **2**, 79–87 (1999).
22. Bastos, A.M. *et al.* Canonical microcircuits for predictive coding. *Neuron* **76**, 695–711 (2012).
23. Eliades, S.J. & Wang, X. Neural substrates of vocalization feedback monitoring in primate auditory cortex. *Nature* **453**, 1102–1106 (2008).
24. Keller, G.B. & Hahnloser, R.H.R. Neural processing of auditory feedback during vocal practice in a songbird. *Nature* **457**, 187–190 (2009).
25. Saleem, A.B., Ayaz, A., Jeffery, K.J., Harris, K.D. & Carandini, M. Integration of visual motion and locomotion in mouse visual cortex. *Nat. Neurosci.* **16**, 1864–1869 (2013).
26. Gavornik, J.P. & Bear, M.F. Learned spatiotemporal sequence recognition and prediction in primary visual cortex. *Nat. Neurosci.* **17**, 732–737 (2014).
27. Xu, S., Jiang, W., Poo, M.-M. & Dan, Y. Activity recall in a visual cortical ensemble. *Nat. Neurosci.* **15**, 449–455 (2012).
28. Shuler, M.G. & Bear, M.F. Reward timing in the primary visual cortex. *Science* **311**, 1606–1609 (2006).
29. Poort, J. *et al.* Learning enhances sensory and multiple non-sensory representations in primary visual cortex. *Neuron* **86**, 1478–1490 (2015).
30. Aghajan, Z.M. *et al.* Impaired spatial selectivity and intact phase precession in two-dimensional virtual reality. *Nat. Neurosci.* **18**, 121–128 (2015).
31. Cho, J. & Sharp, P.E. Head direction, place, and movement correlates for cells in the rat retrosplenial cortex. *Behav. Neurosci.* **115**, 3–25 (2001).
32. Alexander, A.S. & Nitz, D.A. Retrosplenial cortex maps the conjunction of internal and external spaces. *Nat. Neurosci.* **18**, 1143–1151 (2015).
33. Weible, A.P., Rowland, D.C., Pang, R. & Kentros, C. Neural correlates of novel object and novel location recognition behavior in the mouse anterior cingulate cortex. *J. Neurophysiol.* **102**, 2055–2068 (2009).

ONLINE METHODS

Animals and imaging. All experiments were carried out in accordance with protocols approved by the Veterinary Office of the Canton of Basel, Switzerland. For the V1 experiments, we used imaging data from a total of 9 female C57BL/6 mice, aged 75 to 90 days at the start of the imaging series. For CA1 experiments, we used imaging data from a total of 6 female C57BL/6 mice, aged 60 to 80 days at the start of the imaging series and for ACC experiments, a total of 5 female C57BL/6 mice, aged 71 days at the start of the imaging series. All animals were group-housed in a vivarium (light/dark cycle: 12/12 h). Data from two V1 animals with visible *z*-axis motion were discarded. No statistical methods were used to predetermine sample sizes, but our sample sizes are similar to those generally employed in the field. Mice were water-restricted for the duration of the experiment but allowed to drink water *ad libitum* for 1 h per day in addition to receiving water rewards during experiments. Weight of all mice remained above 80% of starting weight (**Supplementary Fig. 9**). Viral injections and window implantation were performed as previously described[20,34]. Briefly, mice were anesthetized using a mix of fentanyl (0.05 mg/kg), medetomidine (0.5 mg/kg) and midazolam (5 mg/kg) for all surgical procedures. For primary visual cortex imaging experiments, a craniotomy was made over visual cortex and AAV2/1-Ef1a-GCaMP6f-WPRE (titer 7.0×10^{10} or 5.0×10^{11} TU/ml) was injected, and the craniotomy was sealed with a 4 mm or 5 mm glass coverslip. For hippocampus imaging experiments, a 3 mm craniotomy was made above either left or right dorsal hippocampus and posterior parts of cortex were aspirated, and AAV2/1-Ef1a-NES-jRGECO1a-WPRE (ref. 35; titer 1.2×10^{11} TU/ml) was injected into region CA1. The craniotomy was sealed with a 3 mm cover slip. For ACC axon imaging experiments, a craniotomy was made over visual cortex and sealed with a 4 mm glass coverslip. Additionally, a small craniotomy over ACC (0.3 mm lateral of bregma) was made and AAV2/1-Ef1a-GCaMP6f-WPRE (titer 1.0×10^{11} TU/ml) was injected before the region was sealed with cyanoacrylate. All viral vectors were injected at a volume of ~150 nl per site. A titanium head bar was attached to the skull and stabilized with dental cement. Imaging commenced 10 to 14 d (primary visual cortex), 23 d (hippocampus) or 30 d (ACC) following injection and was done using a custom-built two-photon microscope[34]. Illumination source was an Insight DS laser (Spectra Physics) tuned to a wavelength of 910 nm. We used a 12 kHz resonance scanner (Cambridge Technology) for line scanning, which enabled frame rates of 60 Hz at a resolution of 400 × 750 pixels. Imaging of ACC axons was performed using an 8-kHz resonance scanner (Cambridge Technology) resulting in frame rates of 40 Hz at a resolution of 400 × 750 pixels. In addition, we used a piezo-actuator (Physik Instrumente) to move the objective (Nikon 16×, 0.8 NA) in steps of 15 µm between frames to acquire images at four different depths, thus reducing the effective frame rate to 15 Hz for the V1 and CA1 experiments and 10 Hz for ACC experiments. Note that the use of different setups for axonal and cell body imaging was the result of lab logistics.

Virtual reality and behavior. The behavioral imaging setup was as previously described[34]. Briefly, head-fixed mice were free to run on an air-supported polystyrene ball, the motion of which was restricted to the forward and backward directions by a pin (**Fig. 1a**). The ball's rotation was coupled to linear displacement in the virtual environment that was projected onto a toroidal screen surrounding the mouse. The screen covered a visual field of approximately 240 degrees horizontally and 100 degrees vertically. All elements of the tunnel including the gratings were calibrated to be isoluminant. Gratings were presented on a uniform gray area once the mouse entered the gray area. A reward zone was located at the end of the tunnel. Reaching the reward zone triggered a 5-s timeout during which the mouse could lick for a water reward provided by a spout located in front of the mouse. After the timeout, the virtual environment reset to the beginning of the tunnel to start the next trial. In early traversals animals were encouraged to run by applying occasional mild air puffs to the neck.

Experimental design. Experimental sessions were 1–2 h long, and each behavioral condition consisted of two such sessions, one per day, spaced on average 24 h apart. Behavioral conditions occurred on subsequent days, with the exception of condition 5 (grating omission), which took place immediately following condition 4. For anesthetized recordings, mice were lightly anesthetized using a mix of fentanyl (0.025 mg/kg), medetomidine (0.25 mg/kg) and midazolam (2.5 mg/kg) at half the surgical dose, head fixed on the setup and allowed to passively view the tunnel, which was presented at a constant visual flow speed. The pre-experience anesthesia condition took place 1 d before condition 1, and post-experience anesthesia took place either immediately after condition 5 or the following day.

Statistics. Nonparametric tests were performed for all analyses (Wilcoxon rank-sum test or Wilcoxon signed-rank test). Paired tests were used where appropriate. No assumptions were made about data distributions in any of the analyses. Further details can be found in the **Supplementary Methods Checklist**, available online.

Data analysis. Imaging data were full-frame registered using a custom-written software[34]. Neurons were selected manually based on their mean fluorescence or maximum projection. This biased our selection toward active neurons. Regions of interest in the axonal data were automatically selected by a combination of independent component analysis and image segmentation as previously described[36]. Fluorescence traces were calculated as the mean pixel value in each region of interest per frame and were then median-normalized to calculate $\Delta F/F$. $\Delta F/F$ traces were filtered as previously described[13]. No blinding to experimental condition was performed in any of the analyses.

Figure 1. For all plots of stimulus-triggered fluorescence changes (**Figs. 1d**, **2b–j**, **3d–g**, **4a–c** and **Supplementary Figs. 4b**, **7a**,**c**,**e** and **8a–c**), fluorescence traces were mean-subtracted in a window 10 to 5 frames (−667 ms to −333 ms for V1 and CA1; −700 ms to −300 ms for ACC) preceding the stimulus onset unless noted otherwise. Neurons were classified as tunnel-responsive if their mean $\Delta F/F$ in a 10-frame (667 ms) window after stimulus onset was at least 1.5% on average for any condition, for any grating or landmark stimulus in the tunnel.

Classification of grating position using neuronal activity was done using Matlab's TreeBagger algorithm. A separate classifier was trained on each condition for each animal. 500 classification trees were used for each classifier. The input to the classifier was the mean $\Delta F/F$ of each neuron for each grating presentation in each traversal within a 10-frame window after grating onset. Traversals were randomly interleaved, and then activity was averaged over three of the randomly chosen traversals at a time. This was done to diminish the influence of trial-to-trial variability on classification. Traversals including an unexpected grating in position 5 in conditions 2 and 4 were omitted from the classification. Classification of spatial position was done as above except that activity was binned into each fifth of the virtual tunnel. For both paradigms, the training set consisted of one half of the randomly interleaved traversals in the condition. The classifier was tested on two randomly selected non-overlapping subsets of the remaining traversals. Performance of the classifier was evaluated as the mean accuracy; i.e., the mean of the diagonal of the confusion matrix for each condition per animal. When determining the effect of traversal speed on classification, we classified traversals with a mean speed of ≤15 cm/s as slow and ≥19 cm/s as fast. For trace deconvolution, traces were first smoothed (mean in a sliding window of 5 frames, or 333 ms). The smoothed traces were then deconvolved using an exponential decay kernel with a time constant $\tau = 0.5$ s. We considered neurons as having stable activity peaks if the peak of each neuron's average activity in each condition was within 5% of tunnel length (5 bins), i.e., one texture length, between conditions.

Selectivity indices for each neuron were calculated using the mean $\Delta F/F$ in the same window after grating onset. Neurons were assigned a selectivity index for a condition if at least one of the responses to a grating (mean A1 + A3 or mean B2 + B4) throughout the condition was at or above 1.5% $\Delta F/F$. Otherwise, selectivity for the condition was set to 0. In **Supplementary Figure 4**, neurons were considered selective if their absolute selectivity index (SI) was greater than 0.5 on average across the animals' experience. To measure stability of selective neurons, we correlated fluorescence traces for each neuron, mapped to spatial coordinates, between traversals. We only included activity in the first 85% of the tunnel to avoid differences due to the variable grating in position 5.

Figure 2. Predictive and visual neurons were sorted based on the position of the peak of their average $\Delta F/F$ after grating-onset over each condition. Predictive neurons were selected as exhibiting a peak within 333 ms (5 frames) of grating onset, and visual neurons were selected as having a peak after 533 ms (8 frames). The window for calculating selectivity index was 133 ms before to 333 ms after grating onset (−2 to 5 frames) for predictive neurons and 533 ms to 1,000 ms (8 to 15 frames) after grating onset for visual neurons. In **Figure 2b**,**c**, the baseline subtraction window for both plots was −1.33 s to −1 s (−15 to −10 frames). To compute the mean of predictive or visual neurons per traversal, the mean of each

predictive neuron was taken in a 7-frame window after grating onset (0 ms to 467 ms), and the mean of each visual neuron was taken within a 8-frame to 15-frame (533 ms to 1 s) window after grating onset. These windows were always used to compute the mean responses for the respective class of neurons in other figures. To compare visually evoked stimulus responses in trials with high predictive activity versus those with high visual activity, we chose presentations with a predictive activity in the top 20th percentile in the 10-frame window following grating onset and compared them to presentations with predictive activity in the bottom 20th percentile. We removed outlying traversals (with average activity values above 3σ from the mean for predictive and visual neuron activity) before making this comparison. In **Figure 2j**, traversals with average predictive activity below median were classified as low-predictive traversals and those above as high-predictive traversals.

Figure 3. In the ACC experiments, animals experienced the same tunnel for conditions 1 through 3. Imaging was only done in condition 1 and 4. To simplify comparison of **Figures 2h** and **3e**, we use B to denote the stimulus the animal saw in position 5 in condition 4. To select for stimulus-predictive ACC axons in **Figure 3d**, we selected predictive axons as in V1 but on the second half of traversals in each condition, and then plotted the responses of the selected axons in the first half of traversals. For this analysis we excluded 2 (of 5) sites with a low number of traversals in the respective conditions. In all other aspects axon selection was identical to neuron selection in the V1 data. To calculate the mean of B-predictive and A-predictive axons in **Figure 3e**, we first mean-subtracted as described above to select neurons and then measured mean activity after a mean-subtraction of 1 s to 500 ms preceding onset.

Figure 4. Omission-selective neurons were selected as having a mean $\Delta F/F$ response larger than 10% to the omission and as having an omission selectivity index larger than 0.33. The omission selectivity index is defined as $SI_{OM} = (R_{OM} - R_{max})/(R_{OM} + R_{max})$, where R_{OM} is the mean response to the omission for each neuron and R_{max} is the largest mean response to any other grating in the tunnel. For statistical comparison of omission-selective neuron activity in traversals with high and low predictive activity (**Fig. 4c**), data were bootstrapped 10 times with random replacement and then a Wilcoxon rank-sum test was performed on the bootstrapped data.

Code availability. All imaging and image processing code can be found online at https://sourceforge.net/projects/iris-scanning/ (IRIS, imaging software package) and https://sourceforge.net/p/iris-scanning/calliope/HEAD/tree (Calliope, image processing software package). Code used for all data analysis is available from the corresponding author upon reasonable request.

Data availability. The data that support the findings of this study are available from the corresponding author upon reasonable request.

34. Leinweber, M. *et al*. Two-photon calcium imaging in mice navigating a virtual reality environment. *J. Vis. Exp.* **50885**, e50885 (2014).
35. Dana, H. *et al*. Sensitive red protein calcium indicators for imaging neural activity. *Elife* http://dx.doi.org/10.7554/eLife.12727 (2016).
36. Mukamel, E.A., Nimmerjahn, A. & Schnitzer, M.J. Automated analysis of cellular signals from large-scale calcium imaging data. *Neuron* **63**, 747–760 (2009).

doi:10.1038/nn.4385